Excess Charge Carrier Injection Densities in PERC Solar Cells at Open-Circuit Voltage and Maximum Power Point

Maksym Tratnikov[1,a)] and Matthias Müller[1]

[1]*Technische Universität Bergakademie Freiberg, Institute of Applied Physics, Leipziger Straße 23, 09599 Freiberg, Germany.*

[a)] Corresponding author: maksym.tratnikov@student.tu-freiberg.de

Abstract. Nowadays passivated emitter and rear contact (PERC) solar cells are mainstream cell technology. An accurate knowledge of the excess charge carrier injection density during illumination will help to understand the kinetic behavior of charge carrier sensitive defects such as boron-oxygen related defect, LeTID defect or FeB pair dissociation and thus supports reliability improvements of PERC cells. However, the excess charge carrier injection density is not easily accessible in experiments. The aim of our research is to investigate the distribution of the injection density in PERC cells in the range of 22% to 24% efficiency. Thus, we perform a numerically simulated Design of Experiment varying the base resistivity and the location of recombination to derive the excess charge carrier injection density. However, no relevant combined influences of the location of recombination on the injection density are found. The base averaged excess charge carrier injection density increases with higher PERC efficiencies as well as with higher specific resistivity of the base. For a sufficient description of the injection density at open-circuit condition, the law of mass action under applied voltage considering high-level injection can be used to calculate the injection density. At maximum power point voltage, an effective voltage at the pn-junction is derived considering the voltage drop due to the lumped series resistance. This effective voltage is used to calculate an injection density with the law of mass action considering high level injection.

INTRODUCTION

An accurate knowledge of the excess charge carrier injection density Δn in solar cells is of high interest for the evaluation of charge carrier injection-dependent defects in silicon, e.g. boron-oxygen-related defect [1,2], LeTID defect [3,4], FeB/Fe_i defect [5]. Those relevant defects change during illumination and/or current injection: FeB pair dissociation to interstitial iron Fe_i, boron-oxygen related defect formation and regeneration (hydrogenation), LeTID defect formation and regeneration. Thus, those defects form and dissociate during Light-/Current-Induced-Degradation (LID/CID) experiments of solar cells and especially during outdoor operation due to changing excess charge carrier injection density. Especially for experimental work and energy yield calculations [6] on defect formation or dissociation in PERC solar cells the excess charge carrier injection density Δn has to be known as Δn determines the reaction rates.

As the newly introduced mainstream solar cell type PERC becomes increasingly efficient, carrier injection sensitive defects are more and more important. Unfortunately, the excess charge carrier injection density is not easily accessible in experiments. Typically, Δn is analytically calculated considering the law of mass action under applied voltage.

This contribution determines the excess charge carrier injection density at 25°C via numerically simulated Design of Experiment (DoE) varying the base resistivity and the location of recombination, i.e. emitter, base or rear surface. We report below on a comparison of numerical simulation results with the commonly used analytical equations for calculating Δn at open-circuit voltage V_{OC} and at the voltage at maximum power point (MPP) V_{MPP} for which we suggest an improved equation considering the lumped series resistance r_{S}.

SiliconPV 2019, the 9th International Conference on Crystalline Silicon Photovoltaics
AIP Conf. Proc. 2147, 020018-1–020018-9; https://doi.org/10.1063/1.5123823
Published by AIP Publishing. 978-0-7354-1892-9/$30.00

ANALYTICAL DERIVATION OF THE EXCESS CHARGE CARRIER INJECTION DENSITY

Carrier injection densities in solar cells can be analytically derived from the law of mass action under applied voltage (diode voltage V_D) by Eq. (1):

$$n \cdot p = (N_\mathrm{D} + \Delta n) \cdot (N_\mathrm{A} + \Delta n) = n_{\mathrm{i,eff}}^2 \cdot e^{\left(\frac{qV_\mathrm{D}}{k_\mathrm{B}T}\right)} \tag{1}$$

where n and p denotes the electron and hole density, N_D and N_A is the donor and acceptor concentration. $n_{\mathrm{i,eff}}^2$ is the effective intrinsic carrier concentration, q is the elementary charge, V_D is the applied (diode) voltage, k_B is the Boltzmann constant and T is the temperature.

Under low level injection (LLI) $\Delta n \ll N_\mathrm{A}$, $p \approx N_\mathrm{A}$, $n \approx \Delta n$, Eq. (1) reduces to Eq. (2) for the cell operating at open-circuit, which is often used for estimating the excess charge carrier density at V_OC.

$$\Delta n@V_\mathrm{OC} \approx \frac{n_{\mathrm{i,eff}}^2}{N_\mathrm{A}} e^{\frac{qV_\mathrm{OC}}{k_\mathrm{B}T}} \tag{2}$$

At MPP Δn is estimated by Eq. (3) as used in Ref. [7].

$$\Delta n@\mathrm{MPP}(N_\mathrm{A}, V_\mathrm{OC}) \approx \frac{n_{\mathrm{i,eff}}^2}{N_\mathrm{A}} e^{\frac{q\left(V_\mathrm{OC} - \frac{k_\mathrm{B}T}{q}\ln\left(1+\frac{qV_\mathrm{OC}}{k_\mathrm{B}T}\right)\right)}{k_\mathrm{B}T}} \tag{3}$$

For the consideration of high level injection (HLI) for p-type wafers $n \approx \Delta n$ Eq. (4) can be derived from Eq. (1) for the V_OC case where only the positive case is reasonable.

$$\Delta n(N_\mathrm{A}, V_\mathrm{OC}) = -\frac{1}{2}N_\mathrm{A} + \sqrt{\frac{1}{4}N_\mathrm{A}^2 + n_{\mathrm{i,eff}}^2 \cdot e^{\left(\frac{qV_\mathrm{OC}}{k_\mathrm{B}T}\right)}} = \frac{N_\mathrm{A}}{2}\left(\sqrt{1 + \frac{4n_{\mathrm{i,eff}}^2}{N_\mathrm{A}^2} \cdot e^{\left(\frac{qV_\mathrm{OC}}{k_\mathrm{B}T}\right)}} - 1\right) \tag{4}$$

NUMERICAL SIMULATION DETAILS

To investigate occurring excess charge carrier injection densities in PERC solar cells, we perform numerical device simulation with TCAD Sentaurus from Synopsys [8] using state-of-the-art physical models [9,10,11] to derive current-voltage characteristics under 1 sun at 25°C. The parametrization of a 24% efficient PERC solar cell (case 15) [12] is taken as a starting point, which features e.g. 10 µm wide front finger and selective emitter, 1 mm front and rear pitch, no busbars and a 2 Ωcm base resistivity. From that we investigate the influence of increased local recombination and changing base resistivity on Δn by a simulated design of experiment (DoE). Thus, the emitter saturation current density $j_{0\mathrm{e}}$, the material saturation current density $j_{0,\mathrm{mat}}$ [7], the rear surface recombination current density $j_{0,\mathrm{rear}}$ and the base resistivity ρ_base are varied systematically in a central composite design of experiment [13]. The main idea of parameter changes is to keep recombination comparable when base resistivity changes. Thus, only saturation current densities are varied which results for base recombination in different SRH lifetime parameters for each base resistivity. TABLE 1 shows the investigated ranges.

TABLE 1. Parameters of the simulated DoE.

DoE	ρ_{base} [Ωcm]	$j_{0\mathrm{e}}$ [fA/cm²]	S_{p} [cm/s]	$j_{0,\mathrm{mat}}$ [fA/cm²]	τ_{n} [µs]	$j_{0,rear}$ [fA/cm²]	S_{n} [cm/s]	$j_{0,sum}$ [fA/cm²]
Minimum	0.5	7	563	12	106/192/1010*	7	5471	26
Central	1.5	37	3845	42	303/527/2013*	27	21009	106
Maximum	2.5	67	7214	72	495/855/3145*	47	36576	186

* Minimum/Central/Maximum for the base resistivity in column two.

$j_{0\mathrm{e}}$ is varied by varying the front surface hole recombination velocity S_{p}, $j_{0,\mathrm{rear}}$ by the rear surface electron recombination velocity S_{n} and $j_{0,\mathrm{mat}}$ by varying the electron recombination parameter τ_{n} of a midgap defect considering the base resistivity ρ_{base} as described above. The hole recombination parameter $\tau_{\mathrm{p}} = \tau_{\mathrm{n}}/1000$ (compare [7]) to neglect injection-dependent effects for our investigations which we don't expect to influence Δn within the idea of our DoE. From the simulation results, we use the following four parameters: efficiency η, V_{OC}, V_{MPP}, the excess charge carrier injection density Δn at MPP and at open-circuit (OC) which is probed in different ways as discussed in the following section.

NUMERICAL SIMULATION RESULTS

Deriving the Excess Charge Carrier Injection Density in the Device Domain

Numerical simulations of solar cells are typically sufficient describing only the smallest irreducible domain. In the case of PERC with line front and rear contacts, it is a two-dimensional domain starting at the center of a front finger and ending at the middle between two front fingers. The domain and the distribution of excess charge carriers in the simulation domain is exemplarily shown in Fig.1 For a better insight into the effect strength, we plot vertical and lateral Δn profiles for different domains (cells) at MPP which are shown in Fig. 2 (Lines C1 to C3).

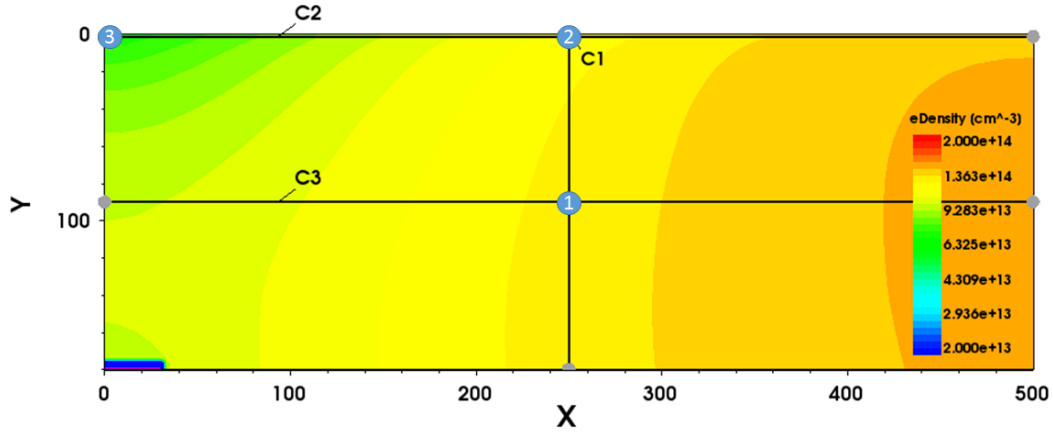

FIGURE 1. Example domain image of the distribution of the electron density at 610 mV which corresponds to the excess charge carrier density Δn@MPP in typical p-type PERC cells.

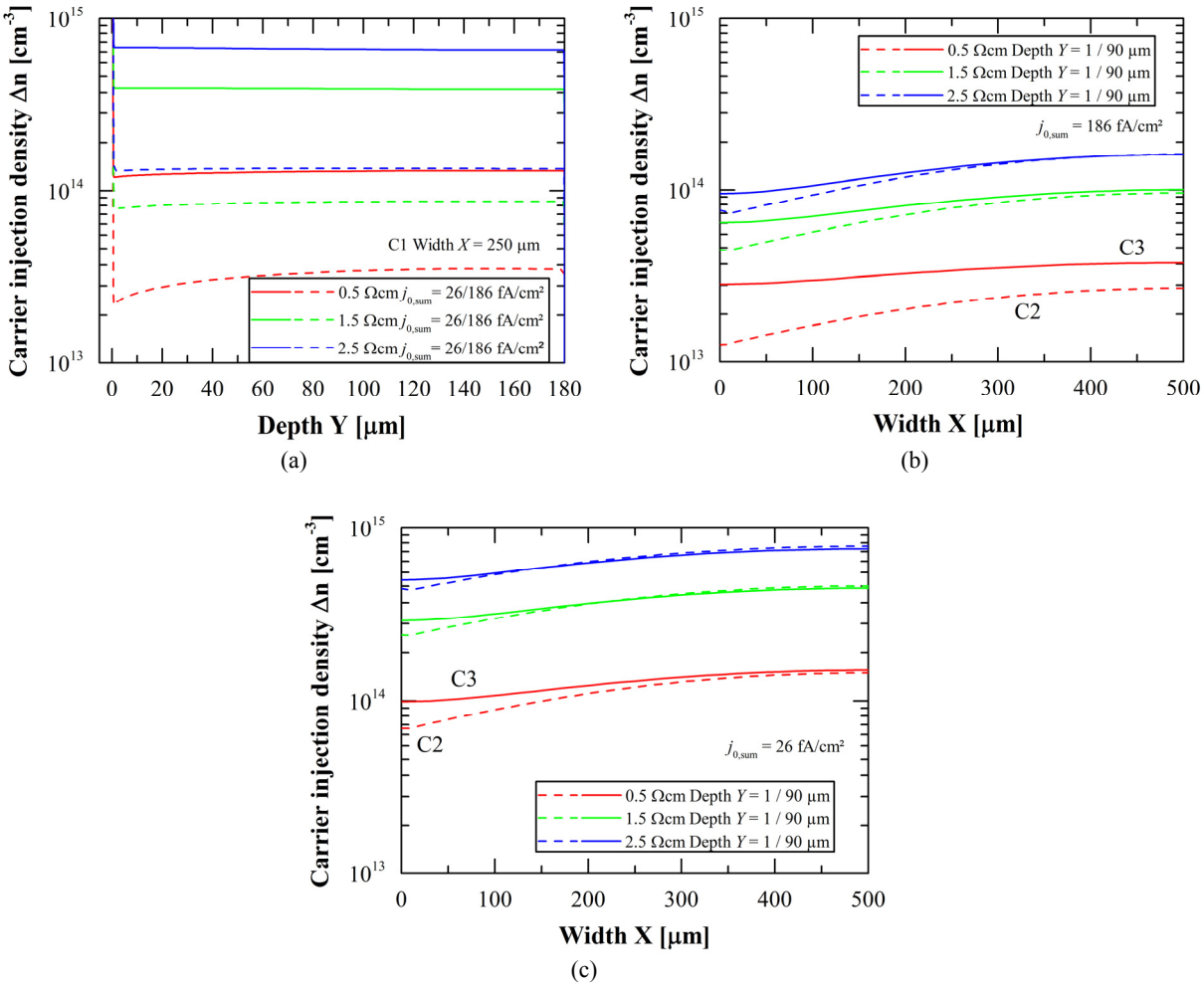

FIGURE 2. (a) Vertical Δn profiles at 250 µm (middle of the domain) width (domain x-axis), (b) and (c) lateral Δn profiles at 1 µm (base side of the pn-junction) and 90 µm (middle of the domain). All profiles are taken at MPP for the best ($j_{0,\mathrm{sum}} = 26\ \mathrm{fA/cm^2}$) and worst ($j_{0,\mathrm{sum}} = 186\ \mathrm{fA/cm^2}$) PERC cell domain for the different $\rho_{\mathrm{base}} = 0.5$, 1.5 and 2.5 Ωcm.

Δn is not constant as Eq. 1-4 might indicate. PERC cells with local front and rear contacts show a lateral and a vertical changing Δn, respectively. Vertical changes are due to the diffusion of the electrons towards the emitter. As rear recombination is sufficiently low in the investigated efficiency range of 22% to 24%, no significant diffusion towards the rear surface is seen in the simulated PERC domains, which would result in lower Δn near the rear surface. Lateral changes in Δn are due to the increasing effective emitter resistance changing the local voltage at the pn-junction at the base side. Additionally, Δn is lower close to front and rear contact due to local contact recombination.

In order to understand, how Δn behaves for the set of simulated PERC cells, we probed it for all simulations at different locations (as denoted in Fig. 1): (1) – center of the domain, (2) – at the middle width of the domain at the base side of the pn-junction, (3) – under the front contact at the base side of the pn-junction, and determined the arithmetic average over the whole base (local back-surface-field excluded). The change of Δn at the voltage at MPP is shown in Fig. 3 for the three base resistivities.

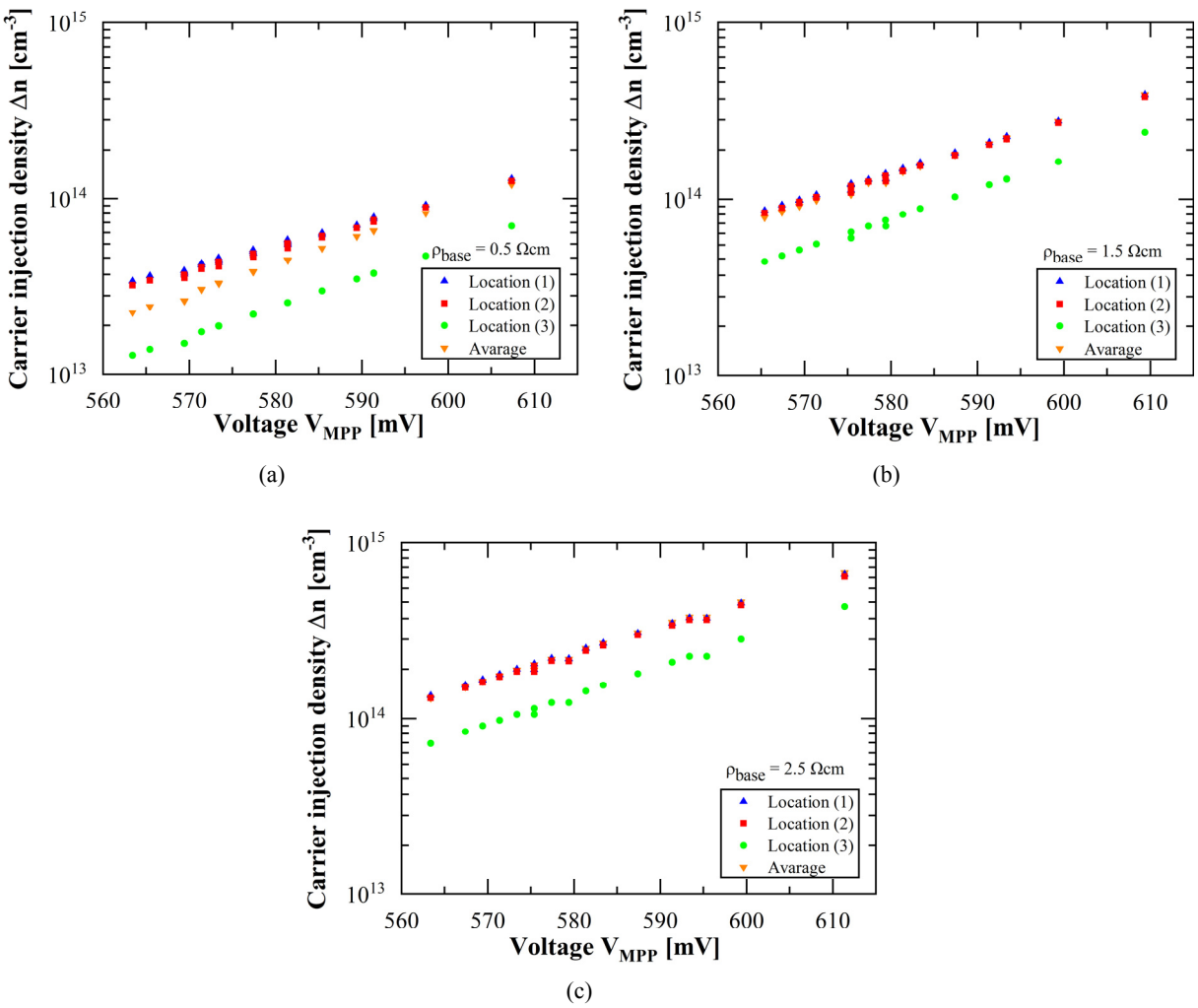

FIGURE 3. Simulated Δn@MPP of the investigated PERC cells at three different locations and averaged over the base for the three base resistivities: (a) 0.5 Ωcm, (b) 1.5 Ωcm, (c) 2.5 Ωcm.

Δn shows in general a continous behavior with increasing V_{MPP} whereas probing at Location 1 and 2 leads to comparable results which show only minor deviation compared to the arithmetic average of Δn in the whole base. Only Δn below the front contact at the base side of the pn-junction differs more strongly due to contact recombination as discussed above.

For the aim of stating a single Δn value for each PERC cell, we consider that it is expected to be used to evaluate defect recombination. Recombination rates are determined by the $n \cdot p$ product. Highest investigated Δn at MPP are about 7×10^{14} cm^{-3} for a base doping of N_{A} of about 5.7×10^{15} cm^{-3} (2.5 Ωcm). Thus, the cells do not face strong high injections effects. Thus, the $n \cdot p$ product reduces to $\Delta n \cdot N_{\mathrm{A}}$ and Δn has a linear influence which would result in a linear influence on the recombination rate allowing to use a arithmetic averaged Δn to consider average base recombination. Therefore, for the following investigations of Δn@MPP and $\Delta n@V_{\mathrm{OC}}$, we will take the arithmetic average of Δn in the base.

Evaluation of the Simulated Design of Experiment

The results of the DoE are analyzed by building a second-order response surface model (RSM) [NIST] where only significant influences are considered ($\alpha \leq 0.05$). The parameter interactions for Δn@MPP are shown in FIG. 4.

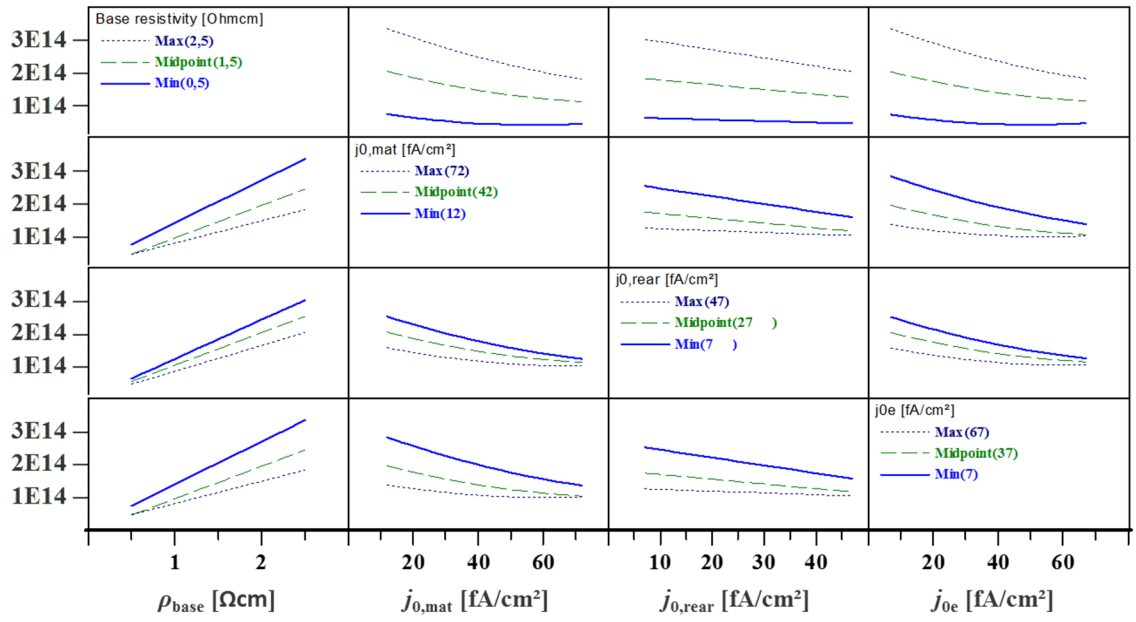

FIGURE 4. Response surface model (RSM) - Interaction graph for Δn@MPP.

No relevant combined influences of the location of recombination on Δn are found. We assume that the strength of recombination at each location is not varied strong enough to significantly introduce interaction. Thus, the simulation results are treated independently of the location of recombination as one similar group of PERC cells. The sum of all saturation current densities $j_{0,\mathrm{sum}} = j_{0e} + j_{0,\mathrm{mat}} + j_{0,\mathrm{rear}}$ becomes the more relevant variable. Therefore, we plot the efficiency against $j_{0,\mathrm{sum}}$ and V_{MPP} for an overview of the results of the design of experiment in Fig. 5.

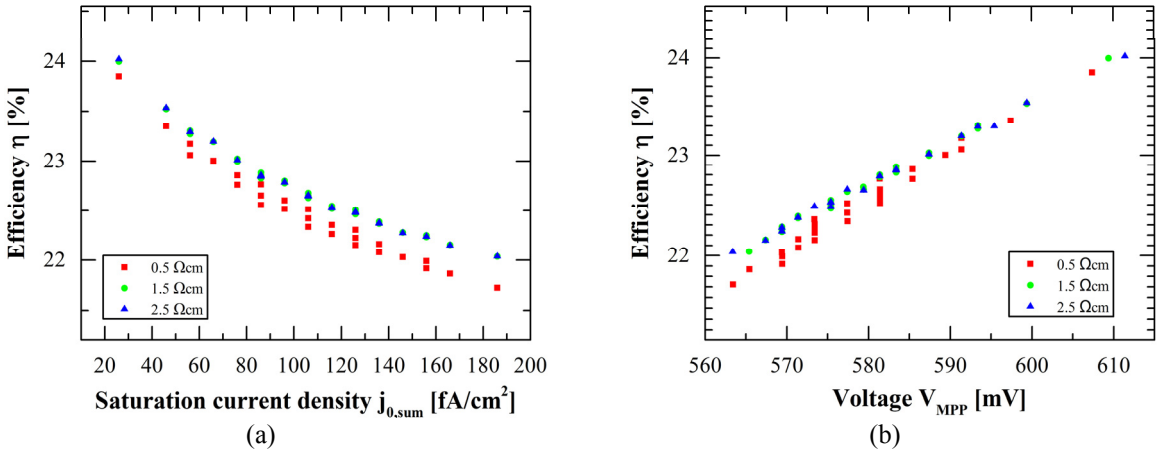

FIGURE 5. Simulated η of the investigated PERC cells for the three base resistivities against (a) the sum of saturation current densities and (b) against the voltage at MPP.

Excess Charge Carrier Injection Density at Open-Circuit $\Delta n@V_{\mathrm{OC}}$

Experimental work on defect formation or dissociation in PERC solar cells is often carried out at open-circuit voltage. Thus, the excess charge carrier injection density Δn is important to be known at V_{OC}. Therefore, we compare our numerical simulations results with the commonly used analytical equations (Eq. 2 and 4) for calculating Δn at V_{OC}. Simulated $\Delta n@V_{\mathrm{OC}}$ in dependence of V_{OC} for the three resistivity values are compared to the Eq. (2) and (4) in Fig. 6.

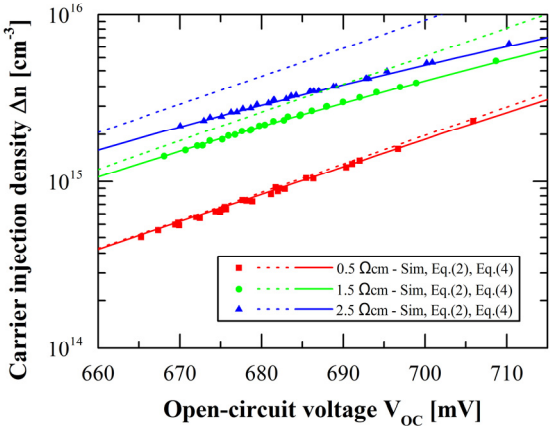

FIGURE 6. Simulated and analytically calculated excess charge carrier injection density at open-circuit $\Delta n@V_{OC}$ depending on open-circuit voltage for three different resistivities.

The excess charge carrier injection density at open-circuit increases with higher resistivity of the wafer and can be well described by Eq. (4) for the resistivity range 0.5 – 2.5 Ωcm at relevant PERC open-circuit voltages. However, Eq. (2) considers only the low level injection case and thus is not sufficient especially for the range of 1.5 – 2.5 Ωcm and higher open-circuit voltages where the high-injection range starts.

Excess Charge Carrier Injection Density at Maximum Power Point Δn@MPP

In order to understand Δn@MPP precisely, the difference between V_{OC} and V_{MPP} is revised. V_{OC} is the case of maximum voltage of a solar cell when the external current of the device is zero. In this case, V_{OC} corresponds to the voltage at the pn-junction V_D. In case of MPP operation, the external current of the device is not zero. Thus, a voltage drop occurs due to the series resistance of the solar cell. The lumped series resistance r_S is used describing an average resistance loss in emitter and base which seems reasonable for our general investigations. At maximum power point, the voltage drop ΔV_{rs} can be estimated by Eq. (5).

$$\Delta V_{rs} = j_{MPP} \cdot r_S \tag{5}$$

where j_{MPP} is the (positive) current density at MPP. Using second Kirchhoff's law for a one-diode-model V_D can be estimated at maximum power point by Eq. (6).

$$V_D = V_{MPP} + \Delta V_{rs} = V_{MPP} + j_{MPP} \cdot r_S \tag{6}$$

Therefore, the excess charge carrier injection densities at maximum power point can be estimated by Eq. (7) combining Eq. (4) and (6).

$$\Delta n(N_A, V_{MPP}, r_S) \approx -\frac{1}{2}N_A + \sqrt{\frac{1}{4}N_A^2 + n_{i,eff}^2 \cdot e^{\left(\frac{q(V_{MPP} + j_{MPP} \cdot r_S)}{k_B T}\right)}} = \frac{N_A}{2}\left(\sqrt{1 + \frac{4n_{i,eff}^2}{N_A^2} \cdot e^{\left(\frac{q(V_{MPP} + j_{MPP} \cdot r_S)}{k_B T}\right)}} - 1\right) \tag{7}$$

Simulated Δn@MPP in dependence of V_{MPP} for the three base resistivities is compared to the analytical calculations using Eq. (3) and Eq. (7) in Fig. 7. Note that r_S is determined by the triple-light-level method [9] evaluated at V_{MPP} using 0.9, 1.0 and 1.1 suns.

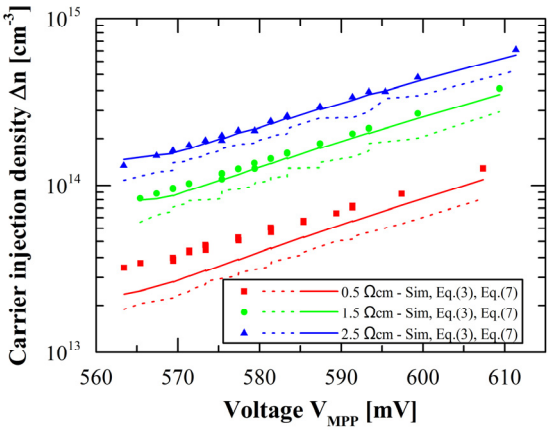

FIGURE 7. Simulated and analytically calculated excess charge carrier injection density at maximum power point Δn@MPP depending on maximum power point voltage for three different resistivities.

The excess charge carrier injection density at MPP increases almost continuously with V_{MPP}, is higher for higher specific base resistivity, and is by about on order of magnitude lower at MPP compared to open-circuit. Deviations in terms of (normalized) root-mean-square deviation (N)RMSD are listed in TABLE 2.

TABLE 2. Deviations of the simulated and analytical calculated Δn@MPP.

Eq.	ρ_{base} [Ωcm]	RSMD [cm^{-3}]	Mean [cm^{-3}]	NRSMD
(3)	0.5/1.5/2.5	2.06/4.17/5.66×10^{13}	5.30/14.9/24.8×10^{13}	39%/28%/23%
(7)	0.5/1.5/2.5	1.19/1.13/1.25×10^{13}	5.30/14.9/24.8×10^{13}	22%/8%/5%

In Fig. 7 the reasonable match between Eq. (7) and the simulated Δn@MPP is well visible. Only for the 0.5 Ωcm PERC cells, a higher deviation is found. In comparison to Eq. (3), Eq. (7) shows a strong improvement in accuracy comparing the (normalized) root-mean-square deviations.

Thus, we recommend to use Eq. (7) for calculating energy yield differences due to Δn affected defects. For experimental work doing MPP tracking under illumination or current induced degradation (CID), we recommend to measure r_{S}, preferable by multiple-light-level method [9]. It is possible to determine Δn at 25°C for typical PERC solar cells using Eq. (7) with the applied voltage, measured current density and r_{S}, the known or measured base doping. Eq. (7) also includes the temperature- and indirectly illumination-dependence of Δn which we assume to generally match but which we haven't validated.

SUMMARY

The knowledge of the excess charge carrier injection density in PERC solar cells is important to evaluate light sensitive defect changes in silicon, e.g. BO-related defect, LeTID defect, FeB pair dissociation. During Light-/Current-Induced-Degradation (LID/CID) experiments of solar cells and especially during outdoor operation those defects form and dissociate.

We determined the excess charge carrier injection density via numerical simulations varying the base resistivity and the location of recombination, i.e. emitter, base or rear surface. No relevant, combined influences of the location of recombination on the injection density at maximum power point are found. An average injection density in the base can be determined although lateral and vertical changes of Δn are apparent in the base.

The comparison of analytical calculations of the injection density at open-circuit voltage of high-efficient PERC cells proves that high-level injection needs to be considered when applying the law of mass action under applied voltage. For a sufficient calculation of the injection density at MPP voltage, we suggest to use the law of mass action under applied voltage considering high-level injection and to correct the external voltage at MPP with the lumped series resistance to derive an effective voltage at the pn-junction, additionally. Our investigation show that it is possible to determine Δn at 25°C for typical PERC solar cells knowing the applied voltage, the measured current density and

r_S, the known or measured base doping. Extrapolations between dark to 1 sun irradiance as wells as realistic outdoor working temperatures seem feasible.

ACKNOWLEDGMENTS

This work was funded by the Federal Ministry for Economic Affairs and Energy (BMWi) under Contract No. 0324274G (project 'GENESIS').

REFERENCES

1. H. Fischer and W. Pschunder, In Proceedings 10th IEEE Photovoltaic Specialists Conference (1973) 404.
2. J. Schmidt, A.G. Aberle, R. Hezel, In Proceedings 26th IEEE Photovoltaic Specialists Conference (1997) 13.
3. K. Ramspeck, S. Zimmermann, H. Nagel, A. Metz, Y. Gassenbauer, B. Brikmann, A. Seidl, "Light induced degradation of rear passivated mc-Si solar cells," in: Proceedings of the 27th EUPVSEC, Frankfurt, Germany, pp.861–865 (2012).
4. F. Fertig, K. Krauß, S. Rein, "Light-induced degradation of PECVD aluminium oxide passivated silicon solar cells," Phys. Status Solidi RRL, pp. 1–6 (2014).
5. A. A. Istratov, H. Hieslmair, E. R. Weber, Appl. Phys. A **69**, pp. 13–44 (1999).
6. M. Müller, M. Ehrl, J. Heitmann, AIP Conference Proceedings **1999**, p. 090002 (2018).
7. M. Müller, Energy Procedia **92**, 138–144 (2016).
8. Synopsys TCAD Sentaurus Device version 2017.06. Synopsys, Mountain View, CA, USA. http://www.synopsys.com
9. P.P. Altermatt, Journal of computational electronics **10(3)**, p. 314–330 (2011).
10. A. Richter, S.W. Glunz, F. Werner, J. Schmidt and A. Cuevas, Physical Review B **86(16)**, p. 165202 (2012).
11. H. Steinkemper, M. Rauer, P.P. Altermatt, F.D. Heinz, C. Schmiga and M. Hermle, J. Appl. Phys. **117(7)**, p. 074504 (2015).
12. B. Min, H. Wagner, M. Müller, G. Fischer, R. Brendel, P.P. Altermatt and H. Neuhaus, IEEE J. Photovolt. **7(6)**, p. 1541–1550 (2017).
13. NIST/SEMATECH, e-Handbook of Statistical Methods, http://www.itl.nist.gov/div898/handbook/ (Accessed 12 June 2019).
14. K. C. Fong, K. R. McIntosh and A. W. Blakers, Prog. Photovolt: Res. Appl. **21(4)**, pp. 490–499 (2011).